

Fractal algorithm for multiple lens analyses

F. ABE¹

¹*Institute for Space-Earth Environmental Research, ISEE, Nagoya University
Furo-cho, Chikusa-ku, Nagoya-shi
Aichi, 464-8601, Japan*

ABSTRACT

A microlensing exoplanet search is a unique method for finding planets orbiting distant stars. However, in the past, the method used to analyze microlensing data could not deal with complex lens systems. The number of lenses was limited three or less. Positions calculations of images and integration of them suffered from severe round-off errors because of singularities. We developed a new algorithm to calculate the light curves of multiple lens systems. In this algorithm, fractal-like consecutive self-similar division (SSD) is used to find sparse images. SSD is also useful for integrating images to efficiently obtain magnifications. The new algorithm does not use root finding for the lens equation and is free from caustic singularities. There is no limit on the number of lenses. Compared to inverse-ray shooting, this method dramatically improves the computing time. The calculation can be adjusted to obtain either a high-precision final result or high-speed quick result. Although this new algorithm was developed for a microlensing planet search, its application to quasar microlensing is also expected. This paper discusses problems in the modeling of a multiple lens system and then presents the new algorithm in detail.

Keywords: Gravitational lenses — Extra solar planets — Quasars — Numerical method and analysis

1. INTRODUCTION

The microlensing planet search method was introduced by Mao & Paczynski (1991). Gravitational microlensing (Einstein 1936; Paczynski 1986) is the magnification of the apparent brightness of a distant star (source star) caused by another star (lensing object) passing in front of the source star. If the lensing object has planets, the perturbations caused by the planets may be observed. The configuration of the planets and host star is obtained by a detailed analysis of the light curve. A collaboration between the microlensing observations in Astrophysics (MOA) project and optical gravitational lensing experiment (OGLE) discovered the first planet (Bond et al. 2004) using this method. Since then, more than 100 planets have been discovered using this method. This method is particularly sensitive (Bennett & Rhie 1996) to the planet orbiting around the Einstein ring radius of the host star. In this region, microlensing is even sensitive to low mass planets that has down to earth mass or less. This region is right outside of the snow line and expected to be the birth place (Ida & Lin 2004) of giant planets. Thus the microlensing planet search is expected to be useful in investigating the formation process of outer planets. In the near future, space telescopes like the Nancy Grace Roman telescope (<https://roman.gsfc.nasa.gov/>) will be used for microlensing planet searches. Because of the improved precision of photometry and cadence of observations, the discovery of numerous planets, including multiple planet systems and exomoons (extra-solar giant natural satellites (Han & Han (2002), Liebig & Wambsganss (2010), Bachelet et al. (2022), Penny et al. (2019))) is expected. However, high-precision photometry and high-cadence observations cause new challenges for analyses, increasing importance of high-precision and high-speed modeling for multiple lens analyses (Bozza et al. (2024)).

Modeling a microlensing event is a well-defined geometrical problem but is challenging. Figure 1 shows a configuration of the multiple lens system. Here we assume that all of the lenses are on the same plane (lens plane). A point on the

lens plane and corresponding point on the source plane are related by the lens equation. This equation for a multiple point lens system is written as follows:

$$\vec{\beta} = \vec{\theta} - \sum_{i=1}^n q_i \frac{\vec{\theta} - \vec{l}_i}{|\vec{\theta} - \vec{l}_i|^2}, \quad (1)$$

where, \vec{l}_i ($i = 1, \dots, n$) is the position vector of the lenses, $\vec{\theta}$ is a position vector on the lens plane, $\vec{\beta}$ is the mapped position vector on the source plane, and q_i is the mass ratio of the i th lens to the total mass. All of the vectors are normalized by the angular Einstein radius:

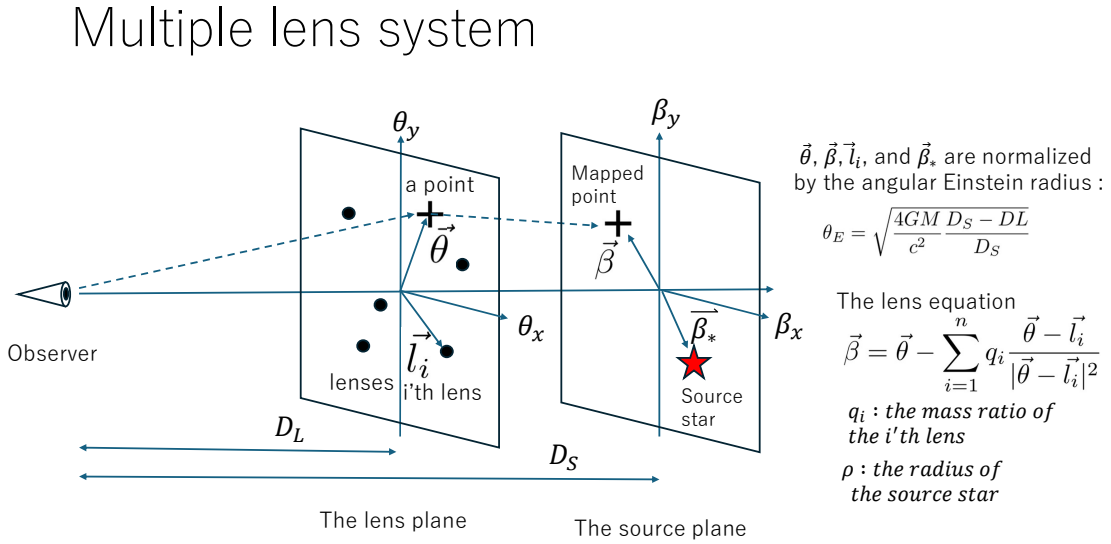


Figure 1. Configuration of the multiple lens system. All of the lenses are assumed to be on a plane (lens plane).

$$\theta_E = \sqrt{\frac{4GM}{c^2} \frac{D_S - D_L}{D_S}}, \quad (2)$$

where, G is the gravitational constant, M is the total mass of the lens system, c is the speed of light, D_S is the distance between the observer and source, and D_L is the distance between the observer and the lens. Although the magnification produced by the lens system can be calculated based on the conservation of the surface brightness, this calculation is not straightforward. A point on the source plane corresponds to multiple points on the lens plane. To find image positions, root finding for the lens equation is necessary. However root finding is difficult for a large number of lenses and sometimes causes severe round-off errors (Bozza et al. (2024)) because of singularities.

During real microlensing events, the source star has a finite size. The shape is circular or slightly elliptical. The images produced by the lens system are deformed and have crescent shapes. Because the surface brightness is conserved during the gravitational lensing, the ratio of the total area of the images to the area of the source star corresponds to the magnification for a uniform surface brightness. In a typical bulge microlensing event, the angular radius of the source star is approximately one micro-arc-second. That is much smaller than the typical angular Einstein radius, which is approximately several hundred micro-arc-seconds. Thus, the produced images are very sparse and small

compared with the angular Einstein radius. Point source approximation has been thought to be effective in obtaining a rough result to begin an analysis. The magnifications of the images for a point source are calculated using the Jacobian. The Jacobian determinant, $J(\vec{\theta})$, is written as follows:

$$\begin{aligned}
 J(\vec{\theta}) &= \begin{vmatrix} \frac{\partial \beta_x}{\partial \theta_x} & \frac{\partial \beta_x}{\partial \theta_y} \\ \frac{\partial \beta_y}{\partial \theta_x} & \frac{\partial \beta_y}{\partial \theta_y} \end{vmatrix} \\
 &= \left[1 - \sum_{i=1}^n q_i \frac{(\theta_y - l_{i,y})^2 - (\theta_x - l_{i,x})^2}{|\vec{\theta} - \vec{l}_i|^4} \right] \left[1 - \sum_{i=1}^n q_i \frac{(\theta_x - l_{i,x})^2 - (\theta_y - l_{i,y})^2}{|\vec{\theta} - \vec{l}_i|^4} \right] \\
 &\quad - \left[\sum_{i=1}^n 2q_i \frac{(\theta_x - l_{i,x})(\theta_y - l_{i,y})}{|\vec{\theta} - \vec{l}_i|^4} \right]^2.
 \end{aligned} \tag{3}$$

Total magnification A is found as follows:

$$A = \sum_{j=1}^m \frac{1}{|J(\vec{\theta}_j)|}, \tag{4}$$

where $\vec{\theta}_j$ is the position of the j th image, and m is the number of images ($n + 1 \geq m \geq n^2 + 1$, depending on the configuration of the lenses). In the region where $J(\vec{\theta}) > 0$, the gravitational lensing produces erect images. On the other hand, in the region where $J(\vec{\theta}) < 0$, the images are inverted. Critical curves are found at the borders of the erect and inverted images where $J(\vec{\theta}) = 0$. Around the critical curves, the images are significantly folded and deformed. The magnification become very high. The critical curves mapped on the source plane are called caustics. As shown in the Eq.3, magnification A diverges to infinity when a point source is on a caustic. This singularity causes a severe problem in the analysis. Around a caustic, a small difference on the source plane causes a large difference on the lens plane. A small error on the source plane is magnified to become a large error if an attempt is made to solve the lens equation to obtain $\vec{\theta}$. Thus calculations with very high precision have been necessary in previous analyses. In the case of high-magnification or sharp caustic crossing events, the finite size of the source star becomes critical. Previous algorithms adopted a step-by-step approach. Initially, the lens equation is solved for $\vec{\theta}$ to obtain the positions of the images. Then, integration's are performed to obtain the total magnification. However, the root finding of the lens equation is difficult. For a single lens ($n = 1$), a simple second order polynomial equation (Paczynski 1986) is derived from the lens equation. For a binary lens event, a fifth order polynomial equation (Witt & Mao 1995) is obtained. Rhie (2002) obtained a tenth order polynomial equation for triple lens system. However, similar algebraic method have not been discovered for more complex lens systems.

Integrating the images is another difficult problem. Bennett (2010) introduced image-centered inverse-ray shooting. In this method a numerous uniform rays are produced on the lens plane and traced to the source plane to integrate the images. As another method, Stokes integration was proposed by Gould & Gauchere (1997). In this method, the boundary points are calculated as roots of the lens equation and the integration uses the Stokes theorem. However, limited inverse-ray-shooting requires significant computation, and a non-uniform surface brightness (limb darkening and/or stellar spots) is hard to handle during the Stokes integration. These calculations must be repeated for different source and/or lens positions to construct light curves. Numerous light curves for various parameters are necessary to compare the results of observations. To analyze a planetary event, the optimum parameters for an extremely large parameter space are necessary. This analysis is very time consuming. Increasing the speed of the integration is critical for a fast analysis.

Another approach to multiple lens analyses is inverse-ray shooting (IRS, Schneider & Weiss (1986), Kayser et al. (1986)). In this method, numerous uniform light rays are produced on the lens plane and traced back to the source plane using the lens equation. The density of the rays on the source plane represents the magnification. Because this method does not use a root-finding approach, there are several advantages compared to conventional methods. There is no limitation on the number of lenses. The finite source effect can easily be implemented, and there is no caustic singularity because this method does not attempt to solve the lens equation. However, this method is not practical for real data analyses because it requires a large amount of computing power for blind shooting numerous rays. The uniform rays must cover all possible areas that including all of the images.

This paper presents a new algorithm for multiple lens systems. This method can be regarded as significant modification of IRS and/or adaptive contouring (?) and does not use the root-finding approach. Thus, there is no limitation

on the number of lenses. Because this method does not attempt to solve the lens equation, there is no critical round-off error problem caused by caustic singularities. Unlike IRS, this method uses a feed-back process to reduce the total calculations. This feed-back can be implemented using a fractal-like self-similar division (SSD) process. The computing time is dramatically reduced using this algorithm.

2. PRINCIPLE

As discussed in section 1, the "no-root-finding" approach has advantages, including a lack of singularities and limitations on the number of lenses. Of course, there are singularities at the centers of the lenses (\vec{l}_i , $i = 1, \dots, n$). But these are not critical. The positions around the centers of the lenses are mapped far from the source. We can simply ignore these singularities. Then, we are free from singularities. The remaining problem is how to reduce the computing time.

Let us consider a point on lens plane $\vec{\theta}$, the corresponding point on source plane $\vec{\beta}$, and a source star centered at $\vec{\beta}_*$. The shape of the source star may be circular, or slightly elliptical. We assume here that we can clearly identify whether $\vec{\beta}$ is inside or outside of the source star. If $\vec{\beta}$ is inside of the source, we can identify $\vec{\theta}$ as inside of an image. If $\vec{\beta}$ is outside of the source, we are not interested in it because it is outside of the images and meaningless when obtaining the total area of the images. If we can produce multiple examples of $\vec{\theta}$ and the corresponding examples of $\vec{\beta}$ we can reproduce the shapes of the images by identifying those examples $\vec{\beta}$ are inside or outside of the surface of the source. Figure 2 shows the distance contours of mapped point $\vec{\beta}$ and the center of the source $\vec{\beta}_*$ ($d = |\vec{\beta} - \vec{\beta}_*|$) on the lens plane. The mass ratios and lens positions are assumed to be, $(q_i, (l_{x,i}, l_{y,i})) = (0.90, (0.0, 0.0)), (0.04, (1.13, 0.11)), (0.04, (0.98, -0.21)), and (0.02, (1.22, -0.22))$. The source position is assumed to be $\vec{\beta}_* = (0.1, 0.0)$. The contours are cropped at $d = 0.1$ to emphasize small values of d . As shown in the figure, the images are clearly identified by the contours. The contours for $d = \rho$ show the images for the source star, where ρ is the angular radius of the source star derived by the angular Einstein radius.

The problem is how to find those images. Of course, a brute-force grid approach wastes time because most of the points are outside of the images. To reduce meaningless computations, we must remove the regions on the lens plane where there is no image. It could be done by identifying regions mapped far from the source.

To identify regions of no interest, we consider a small triangle on the lens plane with the corners: $\vec{\theta}_1$, $\vec{\theta}_2$, and $\vec{\theta}_3$. The corners of the corresponding triangle on the source plane can be calculated to be $\vec{\beta}_1$, $\vec{\beta}_2$, and $\vec{\beta}_3$, respectively. Each corner point can be identified as either inside or outside of the source. If some corners are inside and others are outside, the triangle can be identified as on the edge of the source. If all of the corners are outside, the triangle may be outside of the images. However there is an ambiguity. Because of the gravitational lensing, a triangle on the source plane is deformed and may not be an exact triangle. This effect is expected to be small for small triangles. However, some margins are necessary to securely identify a large triangle. Wide areas can be removed at the beginning of analysis by using appropriate margins. If a triangle is identified as securely outside, we can simply remove it. If the triangle is securely inside, we keep it to calculate the total area of the images. If we can not identify the triangle is inside or outside, it indicate that the triangle is on the border. In this case, we can divide the triangle into smaller ones to more precisely determine the position of the border. Repeating these processes make it possible to determine the shapes of the images. The method we propose here is to repeat fractal-like self-similar divisions to obtain the shapes of the images.

3. ALGORITHM

We invented an analysis algorithm for lens system. In this algorithm, we define pairs of triangles (TriMaps), each of which consists of a triangle on the lens plane (TriL) and corresponding triangle on the source plane (TriS). Then we define three queues of TriMaps: in, out, and uncertain. Figure 3 shows a schematic view of the process. The "in" queue is a collection of TriMaps whose TriSs are securely inside of the source star. The "out" queue is a collection of TriMaps whose TriSs are securely outside of the source star. The "uncertain" queue is a collection of TriMaps whose TriSs are on the border of the source star or not securely identified. Ordinarily, we are not interested in the "out" queue. This queue is only used for the purpose of an integrity check. At the beginning of an analysis, we define a square area to calculate. This area must be large enough to cover all of the images. If the source star is close to or inside of the lens system, the images appear inside or around the Einstein ring θ_E . If the source star is far from the lens system, one of the images appears close to the source. However, the approximate image position can be obtained by a single lens approximation. Then we can define a square area to search the images. To start to search the images,

Contours of d

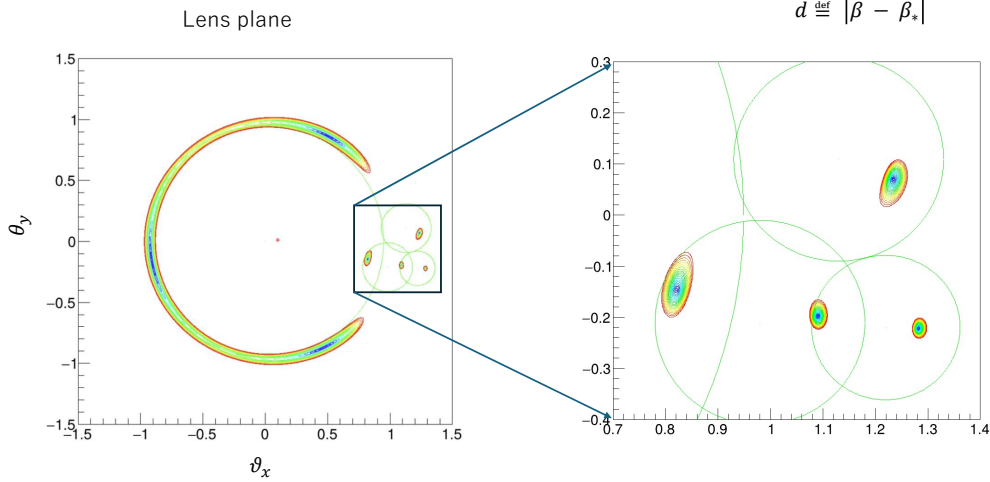


Figure 2. Distance contours of the mapped point on the source plane ($\vec{\beta}$) from the center of the source ($\vec{\beta}_*$) on the lens plane (θ_y vs. θ_x). The left panel shows the total area. The right panel shows the enlarged view around the small lenses. The green circles show individual angular Einstein rings ($\theta_{E,i} = \sqrt{q_i}$). The source position is shown as red asterisk. The contours are cropped at $d = 0.1$ (shown by red) to emphasize small images. Yellow, green, and blue contours show smaller values of d .

we divide the square area into several right angled isosceles triangles as the initial TriLs. Then corresponding TriSs are calculated. First, they are lined up in the "uncertain" queue.

Then we begin the search process to identify the images. The first triangle pair is analyzed to identify whether the TriS is securely in, securely out, or uncertain. If the pair is identified as securely in, the pair is moved to the "in" queue. If the pair is securely out, it is simply removed unless we attempt an integrity check. If the pair is identified as uncertain, the pair is divided into two triangles with similar shapes (right angle isosceles). The new TriL point caused by this dividing process is mapped on the source plane to divide the TriS into two. The new triangle pairs are lined up in the end of the uncertain queue. The same processing is done for all of the initially lined triangle pairs. After this process, all of the triangle pairs become half their original size. We call this consecutive processing a "round". We can repeat this process multiple times to reduce the area of a TriL. As the size of the TriLs decrease, some of the pairs will be identified as in or out. Thus the total TriL area is expected to decrease. If the size of the TriLs in the uncertain queue becomes sufficiently small, all of the images are expected to be picked up.

During these processes, there are three sources of confusion. Confusion is caused by a triangle that is "too large" in size on the lens plane compared to the size of the lens. Just as areas can be inside and outside of the critical curve, the lens system produces images with "opposite" directions. Thus a large triangle around a critical curve may cause confusion. The critical curves occur close to the angular Einstein rings of the lenses ($\theta_{E,i} = \sqrt{q_i}$). To avoid this confusion, a large triangle that is close to a lens is identified as uncertain regardless of whether the corresponding triangle on the source plane is in, out, or uncertain. The second source of confusion appears in the center of a lens. If a triangle includes the lens center, the inside of the triangle is mapped to outside of the corresponding triangle on the source plane. Thus if a small triangle includes the center of the lens and the corresponding triangle on the source plane includes the source star, this pair must be identified as "out". This processing may result in the loss of very small images close to the center of lens. However, the contribution to the total magnification is expected to be very

Selection of triangle pair

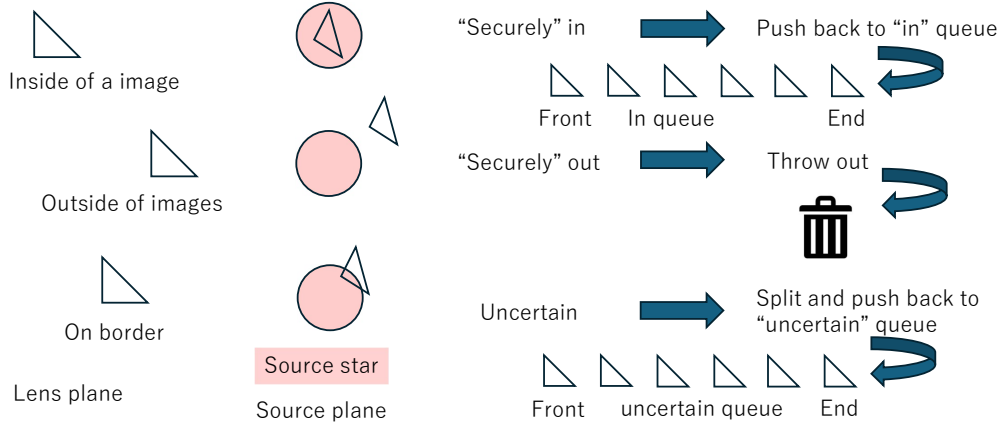


Figure 3. Schematic view of the selection process. There are three queues of triangle pairs (TriMaps): in, out and uncertain. Ordinarily, we do not use those in the out queue. Initially, all of the pairs are listed in the uncertain queue. The first element in the uncertain queue is analyzed and identified as in, out, or uncertain. If the element is in, it is pushed back to the end of the in queue. If the element is out, it is thrown out. If the element is uncertain, it is divided into two TriMaps, which are pushed back to the end of the uncertain queue.

small because those images are very small. The third source of confusion appears when the source is far from the lens system. In this case, a small image appears outside of the source. To pick up this small image, we introduce the single lens approximation to obtain the approximate position of the image and make triangles around it "uncertain" until the image is picked up.

Figure 4 shows the progress of the selection process. Figure 4a shows the triangles on the lens plane before selection. Figures 4b, 4c, and 4d show the same plots after the first, second, and third selections, respectively. The outside areas are gradually increasing and the uncertain areas are decreasing. Repeating these selections, images are found to be "in" triangle areas.

Figure 5 shows the triangles after 15 rounds. Here, we assumed $\rho = 0.01$. The images were reconstructed using "in" and "uncertain" triangles. Figure 5a shows the entire lensing area. Figures 5b, 5c, and 5d show enlarged views of the images. The "uncertain" triangles surrounding the "in" triangles show the border of the images. The lens configuration was the same as that of Fig. 2, which clearly shows all of the images were successfully picked up.

The selection process is still useful after finding images to integrate. If the surface brightness of the source star is constant, magnification A can be obtained based on the ratio of the total area of the images to the area of source star S_s . The total area of the images can be obtained through the summation of the areas of the images. The summation of the areas of the "in" triangles, $\sum_{in} S_i$, gives the lower limit of the total area of the images, where S_i is the area of an "in" triangle. The summation of the areas of the "in" triangles and "uncertain" triangles, $\sum_{in} S_i + \sum_{uncertain} S_i$, gives the upper limit of the total area. The selection process should be repeated to reduce uncertainty. The uncertainty of the total area is expected to decrease as $2^{-n/2}$, where n is the number of repetitions of the selection process. The selection process must be continued until the uncertainty of the magnification becomes sufficiently small. Figures 6a and 6b show the progress in the numbers of triangles and their total area, respectively. The number of "uncertain" triangles

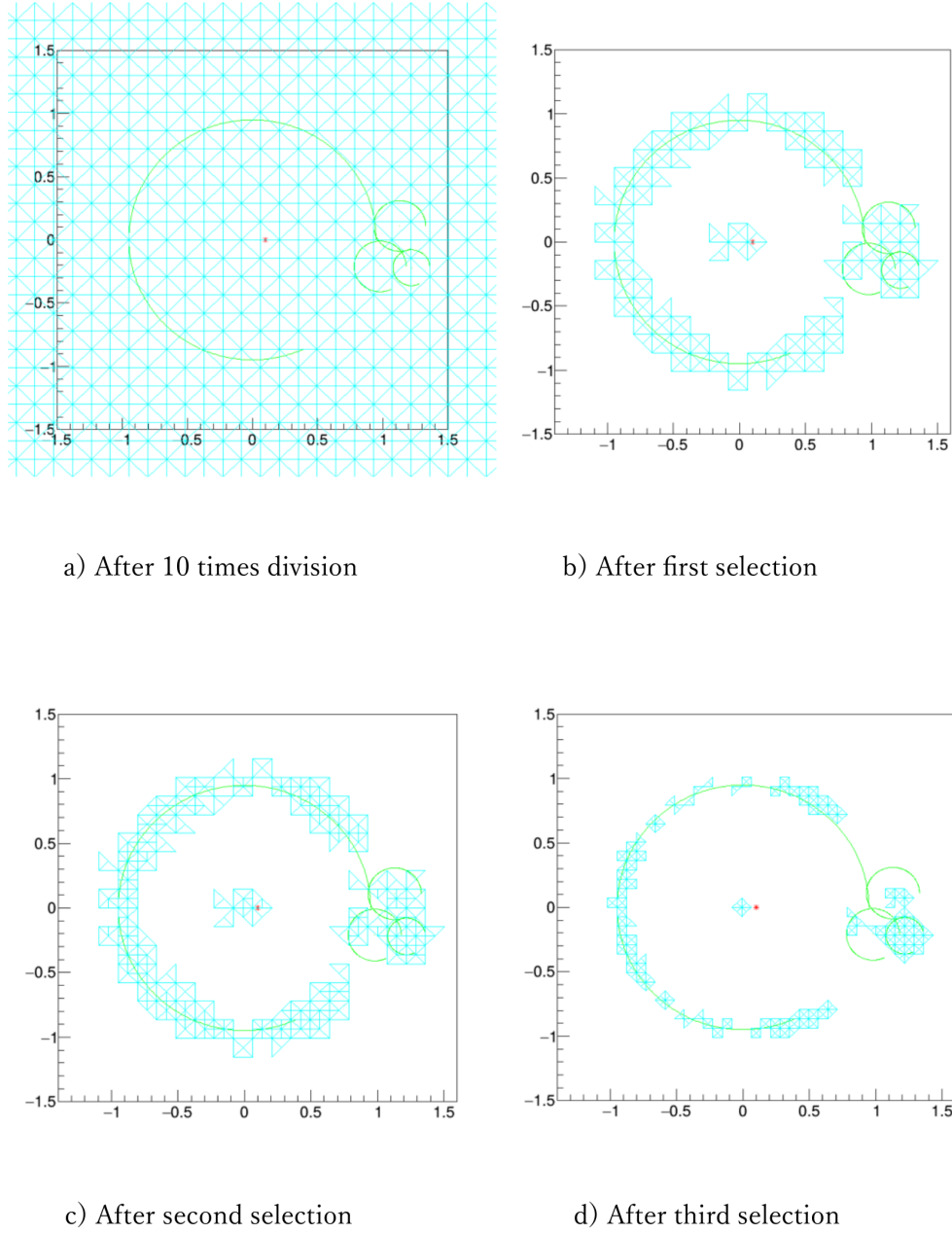


Figure 4. Progress of the selection process. The top left panel (a) shows the triangles on the lens plane before selection. In this stage, there are 2048 triangles on the uncertain queue. The panel b, c, and d show the progress of the selection. The area of uncertain decrease with the selection. But still no in triangle at this stage.

continues to increase with the processing round. The number of "in" triangles also increase after finding the first one. The total area of "uncertain" triangles seems to converge to zero as expected, and the total area of "in" triangles seems to converge to some value. We introduce the first approximation of the total area $S_{IU} \equiv \sum_{in} S_i + \sum_{uncertain} S_i/2$. However S_{IU} does not convergence quickly.

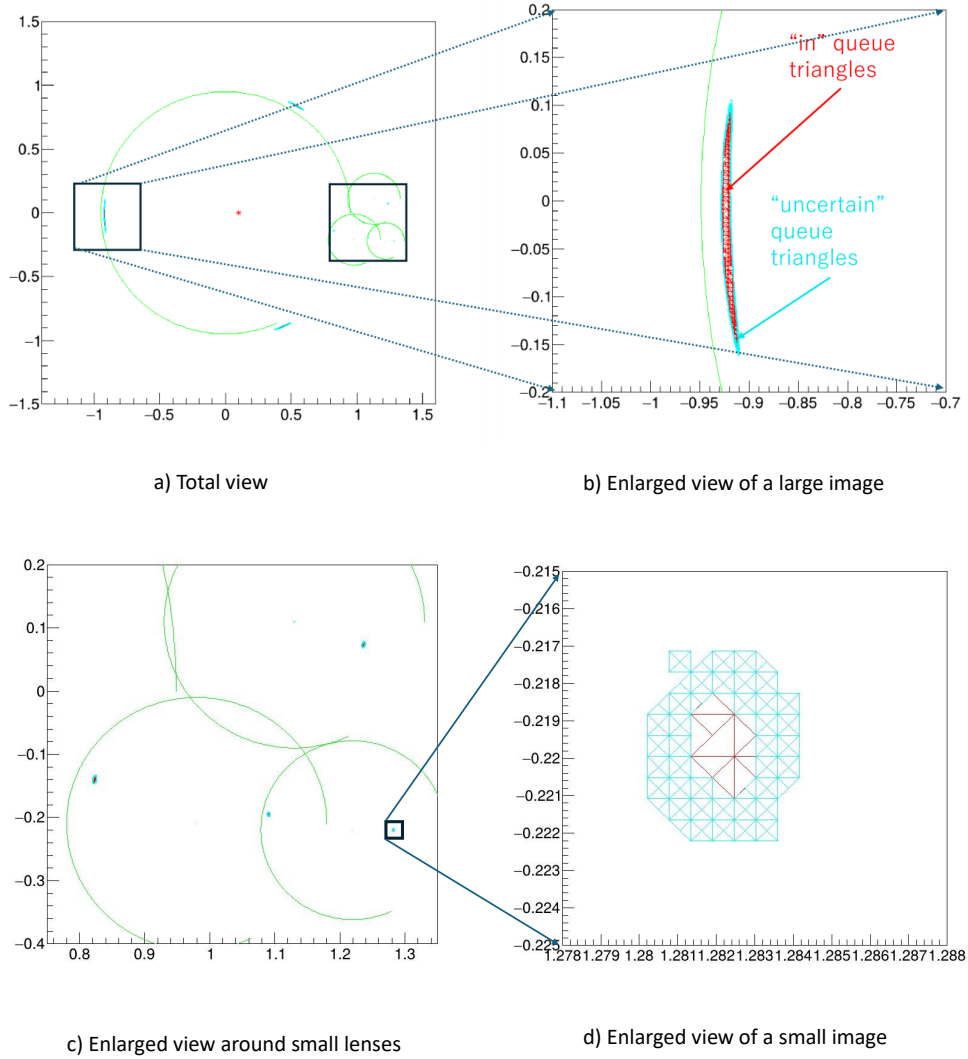


Figure 5. Reconstructed images after 15 times selection.

To improve the convergence speed, we introduced a new approximation. Figure 7 shows the approximation schematically. A portion of the mapped source triangle of an "uncertain" triangle is inside the source star while the remainder is outside. We assumed that the ratios of the inside and outside areas are the same for lens and source triangles. Then we calculated the "in" areas of "uncertain" triangles to obtain a better approximation (S_{sn}) of the total area of the images. Figure 8a shows the difference between S_{IU} and S_{sn} . They appear to be converging to the same value. Figure 8b shows the convergence of the new approximation. In this plot, we assumed that the value after 35 rounds ($S_{sn,35}$) was the correct value, and the differences are plotted. The convergence of the new approximation seemed to be much faster than that of the old one.

A light curve was calculated using this algorithm. Figure 9a shows caustics and the assumed source trajectory. The caustics were obtained as mapped critical curves to the source plane. The critical curves were obtained as high magnification $1/J(\vec{\theta}) \gg 1$ points. However, calculating $J(\vec{\theta})$ with Eq. 3 was found to be very time consuming.

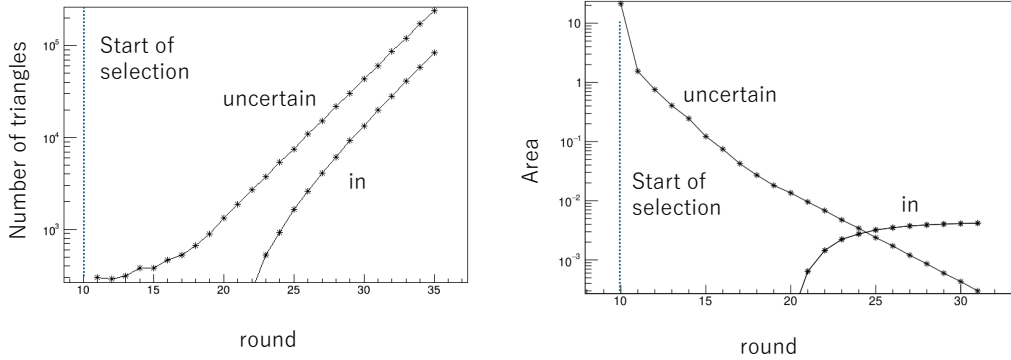


Figure 6. Progress of the total number and total areas of triangles.

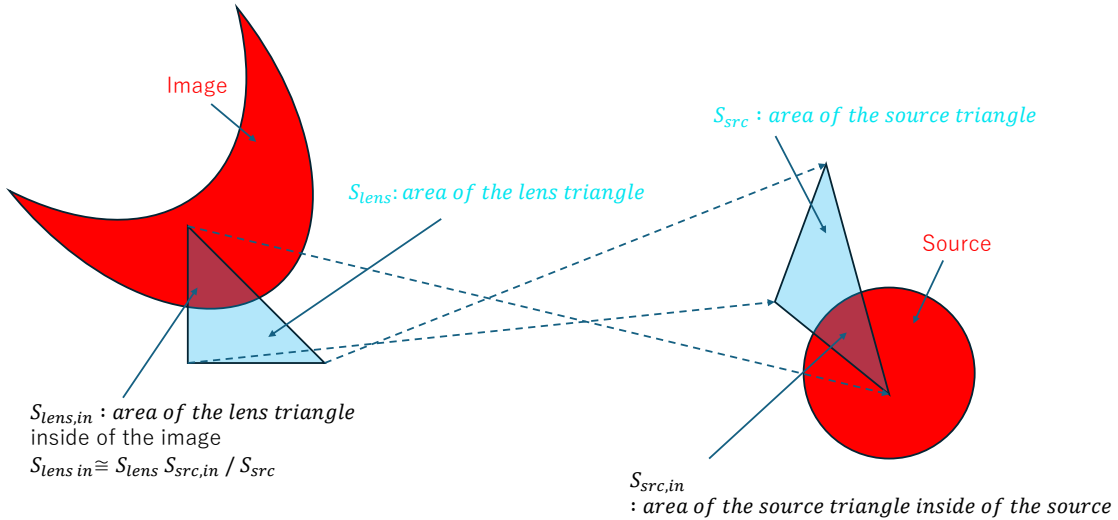


Figure 7. Schematic diagram of the method to obtain better approximation of the total area of the images.

Thus, we used the ratios of the areas of the lens and source triangles instead. Using the assumed source trajectory shown in Fig. 9a and $\rho = 0.01$, we obtained the light curve shown in Fig. 9b. Multiple peaks caused by multiple caustic crossings are clearly shown.

4. IMPLEMENTATION IN C++

We developed a pilot system for the algorithm. This system was implemented in c++. We first used c language to build the pilot system. However we found implementing in c language required significant work. On the other hand, c++ has sufficient functionality to implement complex algorithms. We used class, template, over-

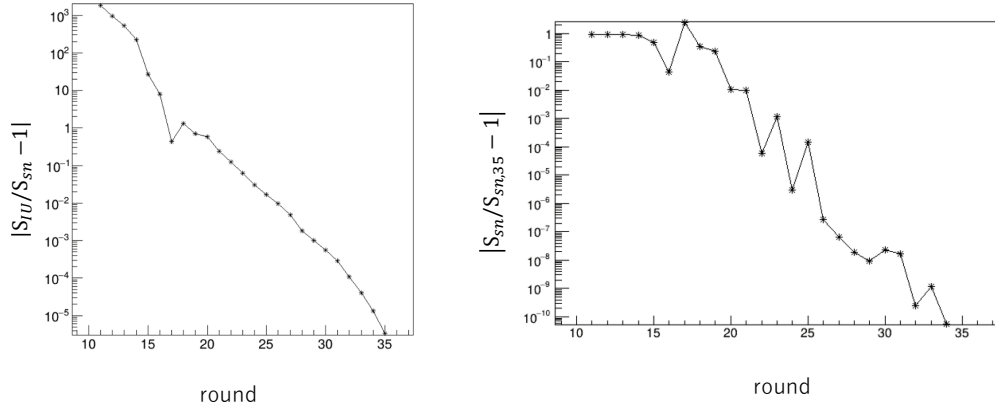


Figure 8. Convergence of the calculated total areas. Difference between S_{IU} and S_{sn} (panel a) and S_{sn} and $S_{sn,35}$ (panel b) vs. round are shown.

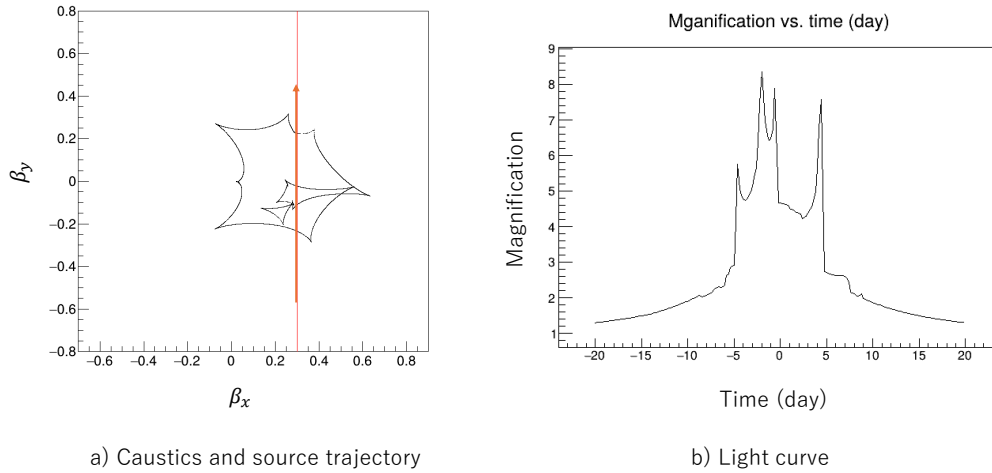


Figure 9. Caustics and source trajectory (a). And light curve (b). The source is assumed to pass (0.3, 0.0) at time 0 and moving to y -direction. The Einstein radius crossing time t_E is assumed to be 20 days.

load, etc to make the pilot system. We also used ROOT class libraries (<https://root.cern.ch/>) and PyROOT (<https://root.cern/manual/python/>) to create graphics and an interface to Python. Although the ROOT class library has significant functionality, we used only to make graphics. Most of the functions of our pilot system could be used without ROOT. The interface to Python with ROOT and PyROOT was very useful. We did not have to make a special definition file. All of the classes and functions in our C++ system can be used from Python.

The source files were organized as conventional header files (.h) and source files (.cpp). The classes and functions were defined in the header and source files. There are 7 pairs of header and source files : Geom, Lens, Source, Fractal, Motion, Lcurve, and RT-Graph. The Geom files defined two-dimensional and three-dimensional geometrical classes and functions. The Lens files defined gravitational lensing classes. The Source files defined the Source classes. The Fractal files defined the classes used in the fractal algorithm. The Motion files defined the classes for motions of the source, lenses, etc. The Lcurve files defined the light curve classes. The RT-Graph files defined the classes used to draw objects. All of the classes except for in the RT-Graph files were defined for the float (32-bit floating point), double (64-bit floating point), and long double (128-bit floating point) types. In our algorithm, calculations are expected to be almost free from singularities. Calculations using the double type are expected to be sufficient for most purposes. The float type could be used to upgrade the program for high-performance computing using inexpensive graphical processing units (GPUs). Recently the inexpensive GPUs used in "gaming PCs" have very high performances for the float type, whereas their performances for the double type are not very high. Calculations using the long double type would be overly precise for most purposes. However it may be useful for a final check of the calculation. In those programs, only RT-Graph uses ROOT class library. Other programs are independent of ROOT.

The current version of the source code is available on <https://github.com/fabe758/Frame>.

5. DISCUSSION

As discussed in section 1, most of the previous methods had a limitation on the number of lenses that could be used. However, the present method can calculate the lensing effect with no limitation on the number of lenses. In principle, the calculation speed is proportional to the number of lenses. Significant CPU power would be needed to fit data because a wide parameter space must be searched to find the best parameters. Although the problem to search large parameters space is still remained, we could overcome most of the problems for the multiple lens analysis. The round-off error problem could also be overcome. Because we do not attempt to solve the lens equation, no caustic singularity appears in the calculation. To test for round-off errors, we performed the same calculations using the float (32-bit floating point), double (64-bit floating point), and long double (128-bit floating points) types and compared the results. The difference was 0.00122% between the float and long double types, and $4.2296608 \times 10^{-14}$ between the double and long double types. Of course, these values depend on the situation. However the result for the double type seemed reasonably good and useful for most purposes, while the float type seemed useful for quickly finding values. In addition to the advantages discussed above, the present algorithm is reasonably fast. We performed benchmark tests using this algorithm with the float, double, and long double types. The light curves for 1000 points were produced in 1.89, 2.17, and 6.60s using the float, double, and long double data types, respectively. Compared to inverse-ray shooting, the CPU times were dramatically reduced. Ordinarily, inverse-ray shooting requires at least several hours to obtain a meaningful magnification map. In this benchmark, we made 15 times selections (round = 25). This corresponded to approximately 4 to 5 digit precision for $\rho = 0.01$. If a higher precision or smaller ρ is needed, additional selections would be necessary. Thus, high-precision or the processing of a small ρ needed longer CPU time. We used an ASUS laptop PC that had an AMD Ryzen AI 9 HX 370 CPU. This is a very powerful machine for a laptop PC. However it is not as fast as a typical server. We used a Linux distribution EndeavourOS running on Windows Subsystem for Linux (WSL). Thus there was some overhead caused by the virtual machine. Although the overhead did not seem to be large, it would be higher for a real performance on a bare Linux. It should also be noted that the present program is single thread, and only one core of the 12 cores was used for this calculation. In principle, the present program could be rewritten for concurrent processing. If 12 cores could be effectively used, the speed would be approximately 10 times faster. If GPUs could be effectively used, a speed increase by a factor of 100 or more could be achieved.

Finding a very small images is a weak point of the present algorithm. Some may be lost. If the source star is far from the lens system, very small images are produced close to the centers of the lenses. Because they are very small, most of them are lost. However, their contribution to the total magnification is expected to be small because they are very small. On the other hand, a small source star produces small images. In this case, additional divisions and selections are necessary. The side length of the lens triangle decreases by a factor of $1/\sqrt{2}$ after division. Thus, seven additional divisions would be necessary to find images produced a source star that was 10 times smaller. To find the equivalent images of source star of $\rho = 0.001$, 22 times selections are needed and it took 8.51, 10.59, 10.59s using the float, double, and long double data types, respectively. In the real microlensing analyses, image sizes varies with time,

fixed number of division would be not appropriate. Probably, stopping divisions with a fixed number of triangle pairs would be more appropriate.

In above discussions, we have focused on the modeling of multiple lens system for microlensing planet search. All lenses are assumed to be on the same plane. But they are not essential. The present algorithm can be easily expanded to analyze more general problems such as quasar microlensing (Kayser et al. (1986)). In Eq.1, we assumed $\sum_i q_i = 1$ and all of the vectors ($\vec{\beta}$, $\vec{\theta}$, and \vec{l}_i) are normalized by θ_E . However, these constraint can be removed. Then, we introduce more general lens equation as,

$$\vec{\beta} = \vec{\theta} - \sum_{i=1}^n m_i \frac{D_S - D_{L,i}}{D_S} \frac{\vec{\theta} - \vec{l}_i}{|\vec{\theta} - \vec{l}_i|^2}, \quad (5)$$

where m_i and $D_{L,i}$ are the mass of the i th lens and the distance to the i th lens from the observer, respectively. Thus, the new algorithm can be applied to quasar microlensing by simply replacing q_i by $m_i \frac{D_S - D_{L,i}}{D_S}$.

6. SUMMARY

In summary, a new algorithm to analyze multiple lens system is introduced. As the algorithm does not attempt to solve lens equation, there is no limitation on the number of lenses and no caustic singularities. This algorithm adopts a fractal-like Self-Similar Division method to reduce the CPU times. Compared to Inverse-Ray Shooting, CPU time is dramatically reduced. The precision of calculation and the CPU time are trade-off. We can obtain quick result by reducing the number of divisions and selections. Increasing the number of divisions and selections, we can obtain more precise values. The precision of the calculation in double is enough for most of the purposes and calculation in float may be even useful for quick result. Although the present program is still on the way to develop and may not be fast enough to search large parameter space to identify multiple planet system, future development and speed-up with parallel processing is expected.

Improving this algorithm and the program will make it possible to explore multiple exoplanet system and search for exomoons in the future space based microlensing observations. The new algorithm is expected to apply future analyses of quasar microlensing too.

- 1 The author would like to thank Professor Valerio Bozza of University of Salerno for his valuable advices and comments.
2 The author is supported by Grant in Aide for Scientific Research, Japan, JSPS 19KK0082.

REFERENCES

- Bachelet, E., Specht, D., Penny, M., et al. 2022, *A&A*, 664, A136, doi: [10.1051/0004-6361/202140351](https://doi.org/10.1051/0004-6361/202140351)
- Bennett, D. P. 2010, *ApJ*, 716, 1408, doi: [10.1088/0004-637X/716/2/1408](https://doi.org/10.1088/0004-637X/716/2/1408)
- Bennett, D. P., & Rhie, S. H. 1996, *ApJ*, 472, 660, doi: [10.1086/178096](https://doi.org/10.1086/178096)
- Bond, I. A., Udalski, A., Jaroszyński, M., et al. 2004, *ApJL*, 606, L155, doi: [10.1086/420928](https://doi.org/10.1086/420928)
- Bozza, V., Saggese, V., Covone, G., Rota, P., & Zhang, J. 2024, arXiv e-prints, arXiv:2410.13660, doi: [10.48550/arXiv.2410.13660](https://doi.org/10.48550/arXiv.2410.13660)
- Einstein, A. 1936, *Science*, 84, 506, doi: [10.1126/science.84.2188.506](https://doi.org/10.1126/science.84.2188.506)
- Gould, A., & Gaucherel, C. 1997, *ApJ*, 477, 580, doi: [10.1086/303751](https://doi.org/10.1086/303751)
- Han, C., & Han, W. 2002, *ApJ*, 580, 490, doi: [10.1086/343082](https://doi.org/10.1086/343082)
- Ida, S., & Lin, D. N. C. 2004, *ApJ*, 604, 388, doi: [10.1086/381724](https://doi.org/10.1086/381724)
- Kayser, R., Refsdal, S., & Stabell, R. 1986, *A&A*, 166, 36
- Liebig, C., & Wambsganss, J. 2010, *A&A*, 520, A68, doi: [10.1051/0004-6361/200913844](https://doi.org/10.1051/0004-6361/200913844)
- Mao, S., & Paczynski, B. 1991, *ApJL*, 374, L37, doi: [10.1086/186066](https://doi.org/10.1086/186066)
- Paczynski, B. 1986, *ApJ*, 304, 1, doi: [10.1086/164140](https://doi.org/10.1086/164140)
- Penny, M. T., Gaudi, B. S., Kerins, E., et al. 2019, *ApJS*, 241, 3, doi: [10.3847/1538-4365/aafb69](https://doi.org/10.3847/1538-4365/aafb69)
- Rhie, S. H. 2002, arXiv e-prints, astro, doi: [10.48550/arXiv.astro-ph/0202294](https://doi.org/10.48550/arXiv.astro-ph/0202294)
- Schneider, P., & Weiss, A. 1986, *A&A*, 164, 237
- Witt, H. J., & Mao, S. 1995, *ApJL*, 447, L105, doi: [10.1086/309566](https://doi.org/10.1086/309566)